

# A VAPID analysis of interstellar lithium in the $\zeta$ Oph sightline

Ian D. Howarth,<sup>1,2★</sup> Richard J. Price,<sup>1★</sup> Ian A. Crawford<sup>1★</sup> and Isabel Hawkins<sup>2★</sup>

<sup>1</sup>*Department of Physics and Astronomy, University College London, Gower Street, London WC1E 6BT*

<sup>2</sup>*Space Sciences Laboratory, University of California, Berkeley, CA 94720-7450, USA*

Accepted 2002 March 22. Received 2002 March 20; in original form 2001 October 12

## ABSTRACT

We present observations of the Li I 6708 Å doublet in the  $\zeta$  Oph sightline, obtained at a resolution of  $\sim 10^6$  and a signal-to-noise ratio of  $\sim 1200$ , together with supplementary observations of K I  $\lambda 7699$  and the Na I  $\lambda 3302$  doublet. These observations marginally resolve the main ‘ $-15 \text{ km s}^{-1}$ ’ system into its two principal clouds; we model the data using standard physical assumptions, but in a statistically rigorous manner, taking fully into account the hyperfine, doublet and isotopic structure for each species, in each cloud, using a new code, VAPID. The average  ${}^7\text{Li}/{}^6\text{Li}$  ratio determined in this sightline is  $1.12 \pm 0.20$  dex (68 per cent confidence interval), in excellent agreement with the solar-system (meteoritic) value. The ratios in the individual clouds are determined with less precision, but are also consistent with the solar-system value, as is the total lithium abundance (with little evidence for depletion). The thermal and ‘turbulent’ broadening in the two clouds is discussed on the basis of observed line widths.

**Key words:** stars: individual:  $\zeta$  Ophiuchi (HD 149757) – ISM: atoms.

## 1 INTRODUCTION

Of the light elements, lithium is of particular interest as a potential diagnostic of conditions in the Universe at the epoch of primordial nucleosynthesis, and of stellar and galactic chemical evolution (e.g. Ryan et al. 2001). The total lithium abundance,  ${}^6\text{Li} + {}^7\text{Li}$ , has been extensively studied in the atmospheres of cool stars, leading to the identification of the ‘Spite plateau’,  $[\text{Li}/\text{H}] \approx -1.1$ ,<sup>1</sup> with the primordial lithium abundance (Spite & Spite 1982a,b). However, the interpretation of stellar abundances relies on relatively complex radiative transfer, and on the degree of processing of photospheric lithium.<sup>2</sup>

The relatively fragile  ${}^6\text{Li}$  isotope is not produced in significant quantities in standard models of big-bang nucleosynthesis, and therefore offers an insight into lithium production processes such as spallation and stellar nucleosynthesis (and hence into the production of other light elements, such as Be and B; e.g., Steigman & Walker 1992; Lemoine, Vangioni-Flam & Cassé 1998; Parizot 2000), and perhaps even into the ingestion of planetary

bodies by stars (Alexander 1967; Israelian et al. 2001). Observationally, the  ${}^6\text{Li}$  abundance is extremely difficult to measure in stellar atmospheres, with only five successful determinations published at the time of writing (e.g. Smith, Lambert & Nissen 1993, 1998; Cayrel et al. 1999; Nissen et al. 1999; Israelian et al. 2001). In general, therefore, the interstellar medium (ISM) offers wider opportunities for testing models of the evolution of lithium abundance through the isotopic abundance ratio. Furthermore, the neutral-atom isotopic ratio  ${}^7\text{Li}^0/{}^6\text{Li}^0$  is insensitive to many potential systematic uncertainties in the determination of absolute lithium abundances, to depletion from the gas phase on to dust grains in the ISM and to uncertainties in ionization fractions, making it a particularly useful diagnostic (e.g. Steigman et al. 1993).

Unfortunately, the only resonance lines accessible from the ground, the Li I  $\lambda 6708$  doublet, are generally rather weak (the dominant ion in the diffuse ISM being  $\text{Li}^+$ ); moreover, the doublet separation is comparable to the isotopic separation ( $\sim 0.15$  and  $0.16$  Å, respectively), so there is inevitably overlap between  ${}^6\text{Li}$  and  ${}^7\text{Li}$  lines. Thus both high resolution and high signal-to-noise ratio are required in order to allow satisfactory modelling. These observational difficulties are reflected in previous (and our own) efforts to measure the  ${}^7\text{Li}/{}^6\text{Li}$  ratio towards  $\zeta$  Oph.

Although there are at least 12 distinct absorption components in this sightline (Barlow et al. 1995; Welty, Hobbs & Kulkarni 1994), more than 90 per cent of absorbers are contained in two clouds at<sup>3</sup>

★E-mail: idh@star.ucl.ac.uk (IDH); rjp@star.ucl.ac.uk (RJP); iac@star.ucl.ac.uk (IAC); isabel@ssl.berkeley.edu (IH)

<sup>1</sup> $[\text{X}/\text{H}] \equiv \log_{10}(\text{X}/\text{H}) - \log_{10}(\text{X}/\text{H})_{\odot}$ ;  $\log_{10}(\text{Li}/\text{H})_{\odot} = -8.7$  by number (Anders & Grevesse 1989), where the subscript ‘ $\odot$ ’ is here to be interpreted as indicating a solar-system (in practice, meteoritic), not solar, value.

<sup>2</sup>Lithium burns in proton reactions above  $\sim 2.5$  MK, so any stellar mixing tends to reduce its surface abundance; the solar-photospheric abundance of lithium is two orders of magnitude less than the meteoritic value, for example.

<sup>3</sup>We quote heliocentric velocities throughout this paper; velocities referred to the dynamical local standard of rest are  $12.20 \text{ km s}^{-1}$  more positive.

–14.0 and –15.0 km s<sup>-1</sup>, and this ‘–15 km s<sup>-1</sup> blend’ is the dominant feature in lithium. Ferlet & Dennefeld (1984) failed to detect <sup>6</sup>Li in this feature, and inferred <sup>7</sup>Li/<sup>6</sup>Li ~ 38 (≥25). Meyer, Hawkins & Wright (1993) subsequently found a very different value, 6.8<sup>+1.4</sup><sub>-1.7</sub>, a result that Lemoine, Ferlet & Vidal-Madjar (1995) criticized as being an average over unresolved components. However, Lemoine et al. in turn failed to model the –15 km s<sup>-1</sup> blend as a close pair of components, even though the velocity structure was already established at the time of their work (Le Bourlet, Gérin & Pérault 1989; Lambert, Sheffer & Crane 1990; Crawford et al. 1994). None the less, in a very thorough study, they concluded that any unmodelled structure was unlikely to affect their results significantly. They derived <sup>7</sup>Li/<sup>6</sup>Li ratios of 8.6 ± 0.8 (±1.4 systematics) and 1.4<sup>+1.2</sup><sub>-0.5</sub> (±1.4) for the –15 km s<sup>-1</sup> blend and –19 km s<sup>-1</sup> cloud, respectively, from spectra with a resolution of 10<sup>5</sup> and a signal-to-noise ratio of 7500 (stochastic). The present work re-examines the ζ Oph spectrum at higher resolution, in an effort to determine improved values for the lithium isotope ratio in this sightline, and to investigate whether the results are consistent with the solar-system (meteoritic) value of <sup>7</sup>Li/<sup>6</sup>Li = 12.3 (Anders & Grevesse 1989).

## 2 OBSERVATIONS

The principal data set discussed here consists of observations obtained during 1994 June, using the ultra-high-resolution facility (UHRF) at the 3.9-m Anglo-Australian Telescope (AAT). The data were extracted in the standard manner using FIGARO routines (Shorridge et al. 1999).

The detector was a Tektronix charge-coupled device (CCD) with 1024 × 1024 × 24-μm<sup>2</sup> pixels. The data have been flat-fielded, but it should be noted that the CCD had good cosmetic properties, and that with UHRF the spectrum is spread over 456 detector pixels in the spatial direction (binned on-chip × 8), which considerably reduces the effects of pixel-to-pixel variations in sensitivity. To mitigate the effects of possible instrumental signatures yet further, 54 separate 1200-s integrations of ζ Oph were obtained in groups of observations with offset central wavelengths. Observations of α Aql and α Vir were obtained to investigate the effect of weak telluric lines; in common with previous workers, we find no evidence that telluric absorption is a significant contaminant of the lithium spectrum.

The total of 18-h integration on the lithium lines yielded a continuum signal-to-noise ratio of ~1200 per wavelength bin, as determined empirically from low-order polynomial fits to the continuum. Supplementary observations of the much stronger K I λ7699 line were obtained at lower signal-to-noise ratio (S/N ratio ≈ 100). The resolution in the reduced spectra, determined from measurements of a stabilized He–Ne laser line, is 0.34 km s<sup>-1</sup> (FWHM,  $R = 8.8 \times 10^5$ ), with the data sampled every 0.16 km s<sup>-1</sup>. In addition, we have used observations of the Na ultraviolet (UV) doublet (λλ3302, 3303) reported by Barlow et al. (1995). Those observations, which have a continuum S/N ratio of ~40, were taken during commissioning of UHRF, before the instrument was fully optimized, and suffer, in particular, from uncertainty in the zero-point of the intensity scale at the ~10 per cent level.

## 3 THE VAPID MODELLING TOOL

We have developed new software to model interstellar absorption lines, under the customary assumptions of a Gaussian line-of-sight

velocity distribution<sup>4</sup> of pure absorbers in each ‘cloud’ (Strömgren 1948). With these assumptions a cloud is fully specified by a central velocity, column density and velocity dispersion. We follow standard practice by giving the column density,  $N$ , in cgs units, and by using  $b$  to characterize the velocity dispersion, where  $b/\sqrt{2}$  is the rms line-of-sight particle velocity (and the rms space velocity for the Maxwellian distribution is  $b\sqrt{3/2}$ ). The FWHM of an unsaturated line is  $2b\sqrt{\ln 2}$ .

The Voigt functions required for the modelling are generated with Lynas-Gray’s VOIGTL routine (Lynas-Gray 1993), and optimization of parameter values is performed with an extensively customized version of Press et al.’s implementation of the Marquadt algorithm (Press et al. 1992). The remainder of the program (~90 per cent of ~6000 lines of code) provides the control logic, user interface, checks, error and statistical analysis, etc. The code is named VAPID, which can be taken to be an acronym for Voigt Absorption Profile (Interstellar) Dabbler.<sup>5</sup>

Operationally, a distinctive feature of VAPID is that it allows cloud parameters to be optimized with respect to several different data sets simultaneously; those data sets may include observations of different transitions of a given species, and may have different S/N ratios and resolutions. Because wavelength calibrations are not of indefinite accuracy, a least-squares adjustment of the velocity zero-points (with respect to a selected reference spectrum) is normally included when optimizing a model with respect to multiple data sets. (This is particularly important for UHRF data sets, where the high dispersion means that only two or three useful lines may be recorded in the calibration arc, with the wavelength accuracy consequently being limited by the reliability of the tabulated arc-line wavelengths.)

The least-squares optimization automatically yields estimates of the uncertainties on derived parameters in the standard way, from the covariance matrix, after data errors have been rescaled to ensure a reduced  $\chi^2$  of unity in regions where the synthesized spectrum falls below a specified residual intensity (0.9999 by default). As is well known, these ‘single-parameter’ error estimates can be significantly smaller than their ‘multiparameter’ counterparts. To obtain realistic, non-parametric error estimates, the analyst may use VAPID to investigate the distributions of parameter values by bootstrap or Monte Carlo methods.<sup>6</sup>

In principle, the bootstrap approach is preferable; in practice, observations often sample interstellar absorption lines rather poorly, encouraging the use of Monte Carlo methods, whereby artificial data sets are generated from the original data and their errors. An advantage of the Monte Carlo approach is that it is straightforward to incorporate additional information (for example, the estimated size of systematic errors in the continuum and zero-intensity levels) when generating the replicated data sets. In practice, our experience (with many data sets in addition to that discussed here) is that the ‘multiparameter’ error estimates are often not more than a few tens of per cent larger than their ‘single-parameter’ counterparts.

The statistical information from an optimization can be used to address two related questions: first, is the fit ‘good’, and secondly,

<sup>4</sup> Consistent with, but not requiring, a Maxwellian three-dimensional velocity distribution.

<sup>5</sup> To dabble is ‘to do anything in a trifling or small way’ (Macdonald 1972).

<sup>6</sup> To be explicit, for a given variable, a ‘single-parameter, 1σ’ error estimate is obtained from the 68 per cent of replicated data sets that give solutions for that variable which are closest to the original least-squares solution; a ‘multiparameter, 1σ’ error estimate is obtained from the 68 per cent of replications which yield the smallest values for  $\chi^2$ .

is the improvement in  $\chi^2$  resulting from the addition of extra components ‘significant’? In each case answers can be obtained by comparing variances, with the  $F$ -test; in the first case,  $\chi^2$  can be compared within and outside the line (where ‘the line’ is chosen to be those regions where the optimized *model* spectrum falls below the continuum).

In the second case, if an initial model with  $n_1$  free parameters yields a chi-squared of  $\chi_1^2$ , and a second model with  $n_2 \equiv n_1 + \Delta n$  free parameters yields  $\chi_2^2$  (where  $\Delta n$  will usually be 3 for each additional cloud), then

$$\frac{\chi_1^2 - \chi_2^2}{\chi_2^2} \frac{N - n_1}{\Delta n}$$

is distributed as  $F[\Delta n, (N - n_2)]$ , where  $N$  is the number of data points in the line. A large value of  $F$  means that the extra terms give a ‘significantly’ improved fit, where the level of significance can be assessed from standard tables of  $F$  (noting that the appropriate distribution is one-tailed; the test is to see whether there is an improvement, not merely a change, in  $\chi^2$ ).

## 4 ANALYSIS: $\zeta$ OPH

### 4.1 Lithium: comparison with previous analyses

We begin by comparing previous models of the lithium lines with our observations; this comparison is made in Fig. 1. Here, as elsewhere in this paper, we take into account hyperfine structure, with the simplification that each doublet component is split into two hyperfine components (thereby neglecting hyperfine splitting of the upper levels). For lithium, we use wavelengths determined by Sansonetti et al. (1995); otherwise, we adopt atomic data summarized by Welty et al. (1994). Unfortunately, Welty et al. do not give primary sources, but their oscillator strengths are identical to those listed by Morton (1991), who does give sources. The wavelengths of Sansonetti et al. for lithium differ from those given by Welty et al. by less than  $0.1 \text{ km s}^{-1}$ .

Meyer et al. (1993, hereinafter MHW) used a single-cloud model and simply fitted appropriately constrained Gaussians to their observations. While this is a reasonable approximation to the profiles of very optically thin lines, such as those considered here, MHW do not give their best-fitting Gaussian parameters, so that their observations are not readily summarized in terms of the usual  $\{v, b, N\}$  triplet. The model shown in Fig. 1 therefore uses the isotopic ratio given by MHW, but with  $v$ ,  $b$  and  $N(^7\text{Li}^0)$  as optimized parameters. Lemoine et al. (1995, hereinafter LFV) parametrized their fit with the standard physical model used here, so only the central velocity of the system,  $v$ , is optimized (to accommodate small velocity zero-point shifts between their observations and ours).

For the purposes of comparison, we have modelled our UHRF observations with a simple single-cloud model; the best-fitting parameters for this model are included in Table 1 (Model Li-1). The resulting  $^7\text{Li}/^6\text{Li}$  ratio,  $1.09^{+0.12}_{-0.10}$  dex, is identical to the solar-system value reported by Anders & Grevesse (1989), and is slightly larger than the values given by MHW ( $0.83 \pm 0.11$ ) and LFV ( $0.93 \pm 0.04$  statistical,  $\pm 0.08$  systematic). The differences are acceptable to within the quoted errors,<sup>7</sup> and are evidently largely

<sup>7</sup> Wherever we report a  $^7\text{Li}/^6\text{Li}$  ratio, the quoted errors are 68 per cent single-parameter confidence bounds from 1000 Monte Carlo simulations. In choosing single-parameter errors we are, in effect, marginalizing ‘uninteresting’ parameters (such as the individual isotopic columns).

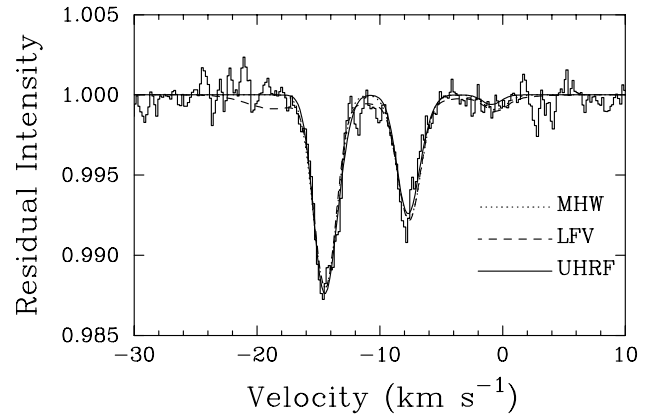


**Figure 1.** Published models of the  $\lambda 6708$  Li lines, compared with UHRF observations. ‘MHW’ denotes Meyer et al. (1993), while LFV denotes Lemoine et al. (1995). In each case, the velocity zero-point of the model has been adjusted by least squares to match best the UHRF data; for the MHW model,  $b$  and  $N$  have also been optimized (while holding the  $^7\text{Li}/^6\text{Li}$  number ratio at the MHW value).

attributable to the  $\lambda 6708.072$  line of  $^6\text{Li}^0$  appearing slightly weaker in our spectrum (central depth  $\sim 99.9$  per cent of the continuum level). Of course, the  $^6\text{Li}^0$  column is additionally constrained by the  $\lambda 6707.921$  doublet component, although that component is irresolvably blended with the hyperfine-split  $\lambda 6707.905$ ,  $6707.917$  doublet component in  $^7\text{Li}^0$ . (In the optically thin limit,  $^6\text{Li}$  reveals its presence by an apparent  $^7\text{Li}$  doublet ratio of less than 2. In our data, that ratio is  $\sim 1.7$ .)

At the level expected from LFV’s modelling, the  $-19 \text{ km s}^{-1}$  cloud is evident in neither our lithium data (which have lower S/N ratio than their observations) nor those of MHW. While there is certainly absorption at this velocity in other species (e.g. Welty et al. 1994; Barlow et al. 1995), it should be noted that there are further features, with comparable column densities in  $\text{Na}^0$  and  $\text{K}^0$ , at  $-12$  and  $-16 \text{ km s}^{-1}$ , and that a single-cloud fit to LFV’s data leaves both positive and negative residuals of similar amplitude ( $\sim 0.04$  per cent of continuum; their fig. 6), possibly as a consequence of very low-amplitude residual fringing in their detector. Furthermore, if the column density of lithium in the  $-19 \text{ km s}^{-1}$  cloud were as large as suggested by LFV, then the implied gas-phase abundance ratio of  $\text{Li}^0/\text{K}^0$  is  $-1.2$  dex – higher by more than 0.5 dex than any sightline in the compilations by Steigman (1996) and Welty & Hobbs (2001).

Irrespective of the lithium column density in the  $-19 \text{ km s}^{-1}$  cloud, the MHW and LFV solutions are essentially indistinguishable in the region of the dominant  $-15 \text{ km s}^{-1}$  blend (and, despite LFV’s criticisms of the MHW fits, yield isotopic ratios that agree to within the joint errors); both agree well with our single-cloud model. We are therefore reassured that the inclusion of any additional components from among the known clouds towards  $\zeta$  Oph has a negligible influence on the results of modelling the  $-15 \text{ km s}^{-1}$  blend; what is of more interest to our discussion is that this feature is properly analysed.

### 4.2 UHRF modelling: lithium ...

The UHRF lithium data can be modelled, independently of all other constraints, with an eight-parameter fit:  $v$  and  $b$  for each of two clouds in the  $-15 \text{ km s}^{-1}$  blend, together with  $N$  for each species in each cloud. We could allow different  $b$  values for each

**Table 1.** Summary of model fits to UHRF data, discussed fully in Section 4. Quoted velocities are heliocentric, and their errors are purely internal, taking no account of possible global zero-point errors (which are considered unlikely to exceed a few tenths of a  $\text{km s}^{-1}$ ). Column densities for potassium are the sum of  $^{39}\text{K}$  and  $^{41}\text{K}$  (in the assumed ratio 1:13.9). Error estimates are 68 per cent single-parameter confidence limits from Monte Carlo simulations. The final column gives the percentage of Monte Carlo simulations that yield lithium isotope ratios equal to or greater (less) than the solar-system value, for least-squares solutions that are less (greater) than that value. Model Li-1 is a single-cloud fit to the  $\lambda 6708$  complex, for comparison with previous analyses. Models Li-2A and 2B are two-cloud fits to the  $\sim 15 \text{ km s}^{-1}$  blend, with and without the isotope ratios as free parameters. Model K-5 is the multicomponent fit to K I  $\lambda 7699$ , and models LiK-5A and 5B are simultaneous fits to both Li and K data (again, with and without the lithium isotope ratios as free parameters). The LiKNa model is a simultaneous fit including the Na  $\lambda 3302$  doublet, with the sodium  $b$  values and columns given in square brackets; model LiKNa' has  $b$  values constrained to be the same for all species. Our recommended solution is model LiKNa.

Model	$v$ ( $\text{km s}^{-1}$ )	$b(\text{K}^0 [\text{Na}^0])$ ( $\text{km s}^{-1}$ )	$\log_{10}N(\text{K}^0 [\text{Na}^0])$ ( $\text{dex cm}^{-2}$ )	$b(\text{Li}^0)$ ( $\text{km s}^{-1}$ )	$\log_{10}N(^7\text{Li}^0)$ ( $\text{dex cm}^{-2}$ )	$\log_{10}N(^6\text{Li}^0)$ ( $\text{dex cm}^{-2}$ )	$\log_{10}\left(\frac{^7\text{Li}}{^6\text{Li}}\right)$	$P$ (per cent)
Li-1	$-14.671 \pm_{0.27}^{0.23}$			$1.32 \pm_{0.04}^{0.04}$	$9.541 \pm_{0.011}^{0.010}$	$8.45 \pm_{0.21}^{0.10}$	$1.09 \pm_{0.10}^{0.12}$	48
Li-2A	$-13.951 \pm_{0.51}^{0.44}$			$1.17 \pm_{0.06}^{0.08}$	$9.097 \pm_{0.011}^{0.018}$	$6.51 \pm_{0.67}^{0.83}$	$2.59 \pm_{0.81}^{0.67}$	2.2
	$-14.983 \pm_{0.27}^{0.16}$			$1.07 \pm_{0.03}^{0.03}$	$9.346 \pm_{0.010}^{0.005}$	$8.427 \pm_{0.048}^{0.099}$	$0.92 \pm_{0.12}^{0.03}$	1.8
Li-2B	$-13.93 \pm_{0.36}^{1.18}$			$1.2 \pm_{0.7}^{1.7}$	$9.09 \pm_{0.31}^{0.06}$	8.00	$\equiv 1.09$	
	$-14.99 \pm_{0.06}^{0.26}$			$1.06 \pm_{0.14}^{0.15}$	$9.35 \pm_{0.05}^{0.13}$	8.26	$\equiv 1.09$	
K-5	$-12.91 \pm_{0.39}^{0.20}$	$0.93 \pm_{0.29}^{0.35}$	$10.32 \pm_{0.14}^{0.18}$					
	$-13.950 \pm_{0.12}^{0.013}$	$0.375 \pm_{0.018}^{0.016}$	$11.401 \pm_{0.023}^{0.018}$					
	$-14.983 \pm_{0.13}^{0.014}$	$0.609 \pm_{0.014}^{0.013}$	$11.655 \pm_{0.011}^{0.009}$					
	$-16.741 \pm_{0.77}^{0.072}$	$0.34 \pm_{0.13}^{0.13}$	$9.821 \pm_{0.088}^{0.073}$					
	$-18.87 \pm_{0.15}^{0.16}$	$1.10 \pm_{0.21}^{0.20}$	$10.069 \pm_{0.070}^{0.064}$					
LiK-5A	$-12.915 \pm_{0.71}^{0.084}$	$0.925 \pm_{0.093}^{0.090}$	$10.323 \pm_{0.034}^{0.027}$					
	$-13.950 \pm_{0.004}^{0.004}$	$0.375 \pm_{0.007}^{0.008}$	$11.401 \pm_{0.004}^{0.005}$	$1.18 \pm_{0.10}^{0.13}$	$9.092 \pm_{0.018}^{0.036}$	$5.59 \pm_{0.47}^{2.02}$	$3.50 \pm_{1.98}^{0.41}$	4.0
	$-14.983 \pm_{0.004}^{0.003}$	$0.609 \pm_{0.006}^{0.005}$	$11.655 \pm_{0.004}^{0.003}$	$1.07 \pm_{0.08}^{0.06}$	$9.349 \pm_{0.018}^{0.010}$	$8.423 \pm_{0.086}^{0.133}$	$0.93 \pm_{0.17}^{0.09}$	3.2
	$-16.741 \pm_{0.54}^{0.049}$	$0.335 \pm_{0.082}^{0.079}$	$9.821 \pm_{0.051}^{0.050}$					
	$-18.87 \pm_{0.11}^{0.10}$	$1.10 \pm_{0.15}^{0.13}$	$10.070 \pm_{0.046}^{0.044}$					
LiK-5B	$-12.91 \pm_{0.39}^{0.20}$	$0.93 \pm_{0.27}^{0.37}$	$10.32 \pm_{0.13}^{0.19}$					
	$-13.950 \pm_{0.11}^{0.012}$	$0.375 \pm_{0.016}^{0.018}$	$11.401 \pm_{0.022}^{0.020}$	$1.19 \pm_{0.20}^{2.11}$	$9.080 \pm_{0.22}^{0.19}$	7.99	$\equiv 1.09$	
	$-14.983 \pm_{0.12}^{0.012}$	$0.609 \pm_{0.013}^{0.012}$	$11.655 \pm_{0.010}^{0.008}$	$1.07 \pm_{0.25}^{0.12}$	$9.36 \pm_{0.20}^{0.11}$	8.27	$\equiv 1.09$	
	$-16.741 \pm_{0.71}^{0.059}$	$0.34 \pm_{0.11}^{0.10}$	$9.821 \pm_{0.075}^{0.069}$					
	$-18.87 \pm_{0.13}^{0.12}$	$1.10 \pm_{0.19}^{0.18}$	$10.070 \pm_{0.062}^{0.054}$					
LiKNa	$-12.91 \pm_{0.13}^{0.11}$	$0.93 \pm_{0.13}^{0.17}$	$10.323 \pm_{0.052}^{0.060}$					
	$-13.950 \pm_{0.005}^{0.008}$	$0.375 \pm_{0.012}^{0.008}$	$11.401 \pm_{0.012}^{0.006}$	$1.18 \pm_{0.12}^{0.21}$	$9.09 \pm_{0.03}^{0.11}$	$4.7 \pm_{1.5}^{3.1}$	$4.4 \pm_{3.1}^{0.4}$	13
		$[0.524 \pm_{0.046}^{0.041}]$	$13.019 \pm_{0.039}^{0.034}$					
	$-14.983 \pm_{0.005}^{0.008}$	$0.609 \pm_{0.006}^{0.009}$	$11.654 \pm_{0.004}^{0.005}$	$1.072 \pm_{0.201}^{0.068}$	$9.351 \pm_{0.052}^{0.023}$	$8.42 \pm_{0.13}^{0.15}$	$0.93 \pm_{0.22}^{0.15}$	6.1
		$[0.828 \pm_{0.014}^{0.014}]$	$13.901 \pm_{0.006}^{0.007}$					
	$-16.741 \pm_{0.70}^{0.066}$	$0.34 \pm_{0.12}^{0.09}$	$9.821 \pm_{0.078}^{0.062}$					
	$-18.87 \pm_{0.13}^{0.13}$	$1.10 \pm_{0.20}^{0.18}$	$10.069 \pm_{0.063}^{0.055}$					
LiKNa'	$-12.60 \pm_{0.19}^{0.26}$	$0.44 \pm_{0.36}^{0.67}$	$10.06 \pm_{0.24}^{0.18}$					
	$-13.947 \pm_{0.38}^{0.035}$	$0.407 \pm_{0.039}^{0.043}$	$11.391 \pm_{0.048}^{0.054}$	0.407	$8.998 \pm_{0.106}^{0.076}$	7.908	$\equiv 1.09$	
		$[0.407]$	$13.325 \pm_{0.084}^{0.089}$					
	$-14.985 \pm_{0.042}^{0.042}$	$0.649 \pm_{0.046}^{0.037}$	$11.665 \pm_{0.046}^{0.037}$	0.649	$9.296 \pm_{0.058}^{0.055}$	8.206	$\equiv 1.09$	
		$[0.649]$	$13.836 \pm_{0.033}^{0.035}$					
	$-16.84 \pm_{0.26}^{0.25}$	$0.17 \pm_{0.21}^{0.41}$	$9.71 \pm_{0.44}^{0.33}$					
	$-18.89 \pm_{0.62}^{0.51}$	$1.06 \pm_{0.65}^{1.05}$	$10.06 \pm_{0.32}^{0.21}$					

isotope, but for purely thermal broadening the values would differ by only 8 per cent (less if any non-thermal broadening is present), and the present data are inadequate to provide discrimination at this level. Furthermore, in principle we should model each separate

observation simultaneously (for example, formally to optimize, rather than simply to measure, velocity offsets between them). In practice, however, the S/N ratio in individual observations is such that the statistical 'best fit' is often physically unacceptable, as the

software locks on to noise features rather than interstellar lines. We therefore simply model the summed spectra (for which the relative wavelength scales are, in any case, good to fractions of a pixel).

Results for the eight-parameter, lithium-only model are given in Table 1 (Model Li–2A). This fit is formally good, in the sense that the null hypothesis of compatible residuals in the line and in the continuum cannot be rejected. However, the two components contributing to the  $-15 \text{ km s}^{-1}$  blend are not resolved (not because of instrumental shortcomings, but because the intrinsic line widths are comparable with the separation), consequently there is a correlation between the line width, the line location and the line strength for each component (while conserving these quantities for the blend). We address this point further in Section 5.1.1.

The most interesting result from the two-cloud fit is that the distributions of solutions from 1000 Monte Carlo replications for the lithium isotope ratios are quite strongly peaked away from the meteoritic value, as indicated by the final two columns of Table 1. Although it should be noted that the final column gives the *one-tailed* probability that the observed value is consistent with the solar-system value (so that the probability that the two values are the same is twice the tabulated statistic), the  $\sim 2\sigma$  differences between inferred and meteoritic isotope ratios clearly merit further investigation.

As a point of reference, we therefore conduct a second two-component fit to the lithium data, in which the isotopic ratio is held fixed at the solar-system value in both clouds (Model Li–2B in Table 1). The resulting model is almost identical to Li–2A, differing by less than 0.0003 continuum units at all wavelengths (that is, expressed in terms of the data errors, by less than  $0.4\sigma$ ). Increasing the number of degrees of freedom by two incurs an increase of  $\sim 10$  per cent in  $\chi^2$ , but with  $F(2, 82) = 0.5$  the two models are, statistically, completely indistinguishable. In other words, the present analysis is consistent with a solar-system lithium isotope ratio in both components of the  $-15 \text{ km s}^{-1}$  blend.

### 4.3 ... potassium ...

As noted above, the lithium data alone do not reliably fix the velocity separation of the two clouds contributing to the  $-15 \text{ km s}^{-1}$  blend. We therefore look to other absorption-line systems for additional constraints. While it is difficult to be certain that any species is distributed strictly cospatially with Li<sup>0</sup>, the other neutral alkali metals are perhaps the most likely to meet this condition, with sodium and potassium the most easily accessible spectroscopically. Any cloud detectable in lithium is virtually certain to be saturated in the well-observed sodium D lines, but the much weaker  $\lambda 3302$  doublet provides a more suitable match in terms of line strength. The K I  $\lambda 7699$  line is also sufficiently weak that it can be used in constructing a model of the distribution of lithium. (K I  $\lambda 4044$ , the analogue of the Na  $\lambda 3302$  doublet, is weaker still, but then suffers the same extreme S/N ratio requirement as Li I  $\lambda 6708$ .)

LFV used the potassium line to assist in interpreting their Li I  $\lambda 6708$  observations; here we go one step further, and simultaneously fit our alkali-metal observations, requiring all species to share the same velocity structure. Because of the uncertainties in the intensity zero level of the UHRF sodium data (cf. Barlow et al. 1995) we begin by considering K I  $\lambda 7699$ . Furthermore, the two components of the  $-15 \text{ km s}^{-1}$  blend are partially resolved in  $\lambda 7699$ , affording a much better determination of the parameters of each cloud.

Like lithium, potassium has two relatively abundant isotopes, <sup>39</sup>K and <sup>41</sup>K, each displaying hyperfine structure.<sup>8</sup> Using the measurements of hyperfine structure given by Bendali et al. (1981), we have conducted model fits to the  $\lambda 7699$  feature, and find that the isotopic ratio for potassium cannot be determined with any useful degree of accuracy from our data. We therefore fix the <sup>41</sup>K : <sup>39</sup>K ratio at the solar-system value of 13.9 : 1 (Anders & Grevesse 1989). We are unaware of any reason to expect significant spatial variations in this ratio, and in any case the corollary of the indeterminacy of the ratio from our data is that the model fits to  $\lambda 7699$  are insensitive to the assumed <sup>41</sup>K : <sup>39</sup>K ratio.<sup>9</sup> The best-fitting model to  $\lambda 7699$  is summarized in Table 1 (model K–5). The tabulated five-cloud model gives a formally significant improvement over a four-cloud model, and is in excellent agreement with the model presented by Welty & Hobbs (2001).

The next step is to fit simultaneously the Li and K data sets, appropriately weighted, allowing these two species to have different *N* and *b* values in each cloud, but requiring them to share the same velocities. As expected, lithium proves to be detected in only the  $-15 \text{ km s}^{-1}$  blend (in all other clouds the derived column is less than the error on the column). The final model is presented in Table 1 (Model LiK–5A), and is a formally good fit to the data, in that the *F*-test gives no indication that the null hypothesis of compatible residuals in the lines and in the continuum can be rejected.

The additional constraint provided by the potassium line has rather little effect on the lithium model (in part because, in practice, we ‘worked backwards’ from the potassium fit when optimizing the lithium solution). The inferred lithium isotope ratios are again suggestive of non-meteoritic values, but, as in the case of lithium-only fits, imposing the solar-system isotope ratio results in a very similar model profile (differences  $< 0.0003$  continuum units); this is Model LiK–5B in Table 1. The conclusion that our data are consistent with a solar-system lithium isotope ratio in both components of the  $-15 \text{ km s}^{-1}$  blend is therefore unchanged by the inclusion of constraints from the potassium line.

### 4.4 ... and sodium

Finally, we include the Na  $\lambda 3302$  doublet in the model. Partly because of their low weight, the sodium data leave the Li/K model almost unchanged (cf. the LiK and LiKNa models in Table 1). The main benefit from their inclusion is, therefore, simply to provide a more objective estimate of the sodium columns and velocity dispersions than was achieved by Barlow et al. (1995). We have also obtained a substantially improved fit, albeit by neglecting additional constraints imposed by observations of the D lines. Barlow et al. discuss the possibility of a third component in the  $-15 \text{ km s}^{-1}$  blend, which appears to be required if a satisfactory fit is to be achieved with the UV and D doublets simultaneously; obviously, improved data would be useful to address this question.

For the fits reported in Table 1, we used Na data adjusted in intensity zero-level as described by Barlow et al. (1995); using unadjusted data decreases  $\log N$  by  $\sim 0.1$  dex and increases *b* by  $\sim 5$  per cent, leaving all other parameters virtually unchanged. The lithium isotope ratio is again consistent with meteoritic values (confirmed by an untabulated model in which the ratio is fixed).

<sup>8</sup> A third isotope, <sup>40</sup>K, is expected to have a negligible abundance: <sup>41</sup>K/<sup>40</sup>K  $\approx 8000$  (Anders & Grevesse 1989).

<sup>9</sup> Fits that assume <sup>39</sup>K = <sup>41</sup>K and <sup>39</sup>K = 0 yield models that are indistinguishable from those listed here.

## 5 DISCUSSION

Overall, the fits provide a posteriori justification for assumption of cospatial distributions of the neutral alkali metals, at least to the extent that satisfactory models are achieved with this assumption. Furthermore, the results are broadly insensitive to detailed assumptions concerning the models; we therefore discuss the results of model LiKNa, the simultaneous solution to all three species (noting where other models give different results).

### 5.1 Line widths

In general, intrinsic interstellar line widths are governed by thermal and ‘turbulent’ broadening (where it is to be understood that ‘turbulence’ is in reality a fudge factor to accommodate any non-thermal velocities), such that

$$b = \left( \frac{2kT_k}{m} + 2v_t^2 \right)^{1/2}$$

for a Gaussian line-of-sight turbulent velocity distribution with rms dispersion  $v_t$ , where  $k$  is Boltzmann’s constant,  $T_k$  is the gas kinetic temperature and  $m$  is the mass of the atom. We can therefore undertake estimates of both thermal and turbulent contributions from the observed line widths for three species in each cloud in the  $-15 \text{ km s}^{-1}$  blend.

#### 5.1.1 Results from unconstrained fits

A simple linear fit to the results of model LiKNa ( $b^2$  versus  $m^{-1}$ , using single-parameter errors from the covariance matrix to estimate weights) yields only upper limits to  $v_t$  of  $<0.26$  and  $<0.32 \text{ km s}^{-1}$  ( $3\sigma$ ,  $-14.0$  and  $-15.0 \text{ km s}^{-1}$  clouds, respectively); this implies subsonic turbulence for gas temperatures  $>20 \text{ K}$ .

The formal gas kinetic temperatures are  $500 \pm 130$  and  $830 \pm 125 \text{ K}$  ( $-14.0$  and  $-15.0 \text{ km s}^{-1}$  clouds). These values are higher than generally found for the diffuse ISM, and are primarily the result of the  $\sim 1 \text{ km s}^{-1}$   $b$  values found for lithium. A somewhat lower temperature,  $390 \pm 210 \text{ K}$ , is obtained for the  $-15.0 \text{ km s}^{-1}$  cloud if the discrepantly broad result for Na is ignored (on the basis of the problematical line fits discussed by Barlow et al. 1995). Including the results for  $\text{Fe}^0$  given by Barlow et al. introduces negligible changes to these results, which are sensitive primarily to the light elements.

There is an obvious potential trade-off between the separation of the two main components in the  $-15 \text{ km s}^{-1}$  blend and their  $b$  values. Because the components are intrinsically unresolved in lithium, the main ‘leverage’ on  $b$  comes from the line width, so that if the velocity separation (constrained mainly by the K line) is larger than found here, the inferred line width (and  $T_k$  values) would be smaller. There are hints that the separations found for molecular lines are indeed slightly larger than our value (e.g. Lambert et al. 1990), but other neutral atomic species are consistent with our result (e.g. Barlow et al. 1995).

To check this, we worked out solutions to the lithium data with the cloud separation fixed at values in the range  $1.00$ – $1.30 \text{ km s}^{-1}$ . These constrained least-squares solutions give best-fitting  $b$  values that are almost constant at  $\sim 1.0 \text{ km s}^{-1}$  for the  $-15.0 \text{ km s}^{-1}$  cloud, and monotonically decreasing from  $\sim 1.2$  to  $\sim 0.5 \text{ km s}^{-1}$  with increasing separation in the  $-14.0 \text{ km s}^{-1}$  cloud. For comparison, Crawford et al. (1994) and Lambert et al. (1990)

estimate  $b$  values for CH of  $0.50$  and  $0.44 \text{ km s}^{-1}$  ( $-14.0 \text{ km s}^{-1}$ ) and  $0.58$  and  $0.75 \text{ km s}^{-1}$  ( $-15.0 \text{ km s}^{-1}$ ), while Crawford & Williams (1997) find  $0.33$  and  $0.91 \text{ km s}^{-1}$  for NH; for purely thermal broadening, the lithium lines should be  $\sim 1.4 \times$  wider – as observed.

#### 5.1.2 Fits with $b$ values constrained

While the foregoing discussion suggests that the line width (and implied high kinetic temperature) is apparently reasonably well established, at least for the  $-15.0 \text{ km s}^{-1}$  cloud, a determination of the kinetic temperatures from  $\text{C}_2$  molecules in this sightline indicates  $\sim 20$ – $30 \text{ K}$ , for each of the dominant clouds (Crawford 1997). If the kinetic temperature appropriate to the neutral alkali metals were this low, then the line widths would be dominated by turbulence, with the implication that the line-width analysis has led to incorrect results. We are therefore motivated to investigate the consequences of assuming turbulence-dominated line widths.

To do this, we conduct fits with the  $b$  parameter constrained to be the same for each species in a given cloud. An illustrative result for a model with the lithium isotope ratio fixed at the solar-system value is listed in Table 1 (model LiKNa’) and shown in Fig. 2. The  $b$  values are  $0.41 \pm 0.04$  and  $0.65 \pm 0.04 \text{ km s}^{-1}$  in the  $-14.0$  and  $-15.0 \text{ km s}^{-1}$  clouds (cf.  $0.65 \pm 0.08$  and  $0.35 \pm 0.07 \text{ km s}^{-1}$  estimated for  $\text{C}_2$ ).

Fits with  $b$  values constrained in this way provide significantly poorer matches to the data, primarily because the ‘shoulders’ of the modelled lines, where they approach the continuum, are too narrow compared with the observed profiles. The  $F$  test indicates that the constrained- $b$  fits are worse than those in which the  $b$  values are allowed to vary, with  $>99.9$  per cent confidence. Either this formal result is misleading (for example, the neutral alkali metals may not be distributed cospatially, as assumed), or the kinetic temperature for the species investigated here is greater than the  $\text{C}_2$  excitation temperature.

## 5.2 Li/K ratios

The modelled column densities yield the gas-phase  $\text{K}^0/\text{Li}^0$  number ratios directly. The column-weighted ratio in the  $-15.0 \text{ km s}^{-1}$  blend is  $\sim 2.27$  dex, summed over isotopes, while the values in the individual clouds are  $\sim 2.30$  ( $-14.0 \text{ km s}^{-1}$ ) and  $\sim 2.25$  dex ( $-15.0 \text{ km s}^{-1}$ , with uncertainties of  $\sim 0.1$  dex). These values compare well with data compiled by Steigman (1996, averaging 2.43 dex) and by Welty & Hobbs (2001; 2.27 dex, range 1.8–2.5).

Conversion from gas-phase neutral-atom abundance ratios to element abundance ratios requires allowance for unobserved ionic species, and for depletion on to grains. Steigman (1996) discusses these issues, finding that

$$\log_{10}(\text{K}/\text{Li}) = \log_{10}(\text{K}^0/\text{Li}^0) - 0.55 \pm 0.08$$

in the gas phase, implying  $(\text{K}/\text{Li}) \approx 1.72$  dex by number, in each cloud. This ratio is in good agreement with the solar-system ratio ( $1.82 \pm 0.05$ ; Anders & Grevesse 1989).

## 5.3 Li abundance and depletion

If we write the fractional abundance of neutral lithium in the gas phase as

$$\mathcal{F} = (\text{Li}^0/\text{Li})_{\text{gas}},$$

the total (gas + dust) interstellar abundance with respect to neutral

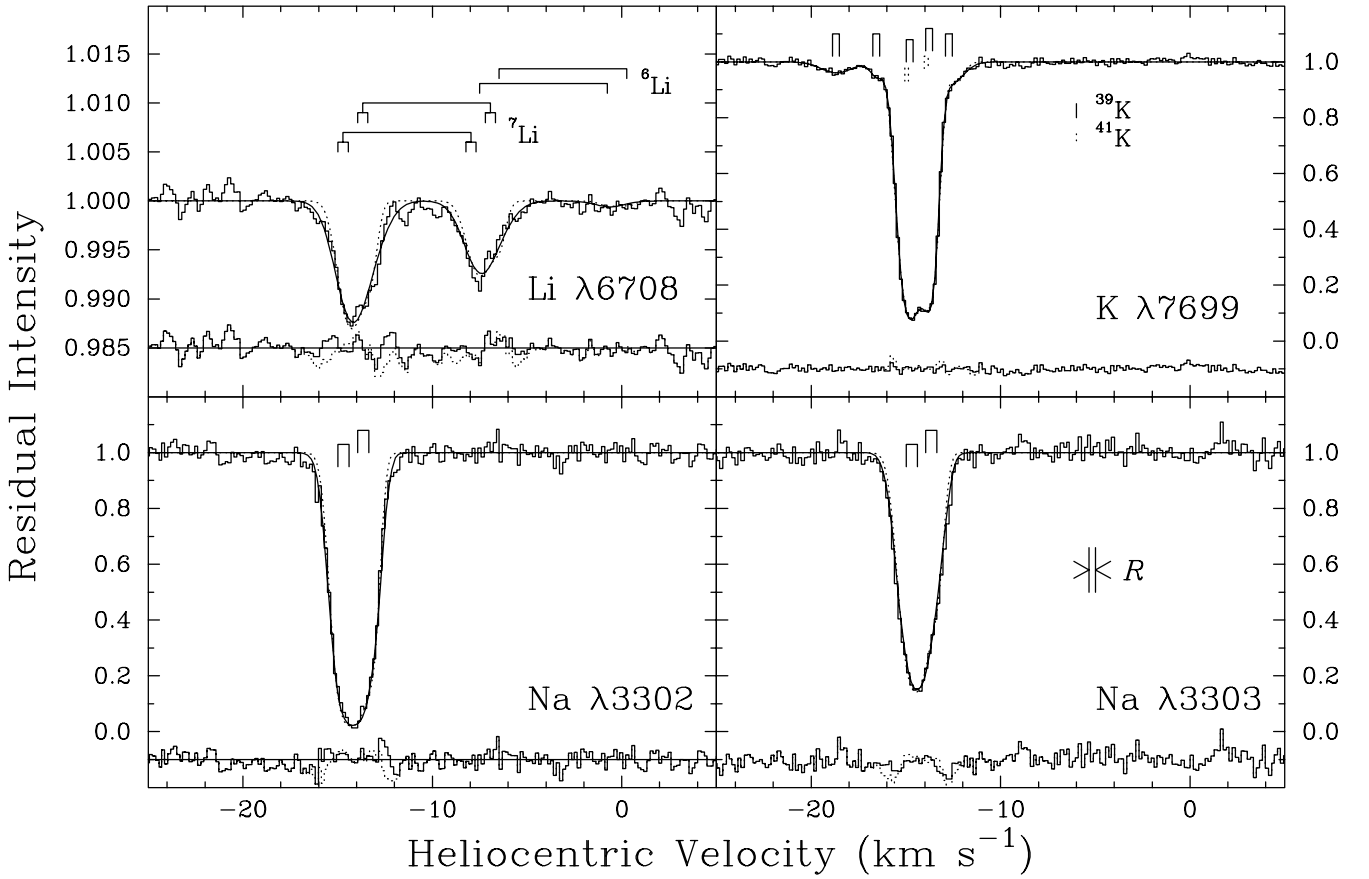


**Figure 2.** VAPID fits to observations of interstellar absorption lines towards  $\zeta$  Oph. The data are plotted ‘histogram’ style; the continuous solid line shows model LiKNa, and the dotted line model LiKNa’ (see Table 1 and Section 5). (O-C) residuals are shown with offset intensity zero-points. Locations of the  $-14.0$  and  $-15.0$   $\text{km s}^{-1}$  clouds are shown in each panel, with hyperfine components indicated by ‘croquet hoops’. Lines of  $^{39}\text{K}$  are shown for all five clouds modelled in the  $\lambda 7699$  feature (with  $^{41}\text{K}$  indicated, by dashed ‘hoops’, for only the two clouds with the largest columns). The resolution of the data is shown in the Na  $\lambda 3303$  panel (‘R’). Note the expanded vertical scale for the lithium feature.

hydrogen as

$$A = N(\text{Li})_{\text{tot}}/N(\text{H}^0),$$

and the gas-phase depletion factor as

$$\delta_{\text{Li}} = N(\text{Li})_{\text{gas}}/N(\text{Li})_{\text{tot}}$$

then the observed column-density ratio in the neutral gas is

$$\frac{N(\text{Li}^0)}{N(\text{H}^0)} = \mathcal{F}\delta.$$

The interstellar neutral-hydrogen column towards  $\zeta$  Oph is  $\sim 20.8$  dex  $\text{cm}^{-2}$  (e.g. Shull & van Steenberg 1985), whence  $N(\text{Li}^0)/N(\text{H}^0) \approx -11.2$  dex. If we assume a ‘cosmic’ ratio of  $N(\text{Li})/N(\text{H}) \approx -8.7$  dex (Anders & Grevesse 1989), then  $\log \mathcal{F}\delta = -2.5$  (with an uncertainty of  $\sim 0.1$ ); that is, only one lithium atom in  $\sim 300$  is present as a gas-phase neutral atom in the  $\zeta$  Oph sightline, the remainder being ionized, incorporated into grains or both.

Any estimate of absolute lithium abundances is therefore highly uncertain, because the corrections for unobserved components are both large and sensitive to local conditions. Encouraged by our referee, however, we compare our value for  $\log \mathcal{F}\delta$  with estimates

of  $\mathcal{F}$  obtained from simple ionization-balance calculations:

$$\mathcal{F}^{-1} = \frac{\text{Li}}{(\text{Li}^0)_{\text{gas}}} \approx \frac{\Gamma(\text{Li}^0)}{\alpha(\text{Li}^+)n_e}, \quad (1)$$

where  $\Gamma(\text{Li}^0)$  is the photoionization rate for  $\text{Li}^0$  and  $\alpha(\text{Li}^+)$  is the radiative recombination rate for  $\text{Li}^+$ . The electron density in the line-forming region,  $n_e$  (assumed to be constant), may in principle be estimated from the ratio of column densities for neutral and first (dominant) ionization stages of an appropriate element, by application of equation (1), *mutatis mutandis*, to that element, but suitable observations do not exist with the resolution required to provide values for each of the two dominant clouds. Furthermore, the photoionization rates  $\Gamma$  are liable to depend on the distances of the clouds from  $\zeta$  Oph. These factors exacerbate already large uncertainties in  $\mathcal{F}$  values derived from data summarized by Morton (1975) and by White (1986). (The major source of the difference between these authors is in their inferred electron densities. Both authors adopted similar atomic data, and similar ionization rates, each based on a *mean* diffuse radiation field. If the ionizing radiation field is enhanced by proximity to  $\zeta$  Oph, then the ratio  $\text{Li}/\text{Li}^0$  is increased.)

Morton’s data yield  $\mathcal{F}^{-1} \approx 30$  for the integrated column in the  $-15$   $\text{km s}^{-1}$  blend. Since  $\delta$  must be  $\leq 1$ , if  $\log \mathcal{F}\delta \approx -2.5$  then Morton’s estimate of  $n_e = 0.7$   $\text{cm}^{-3}$  must be too large, his adopted

value for the photoionization rate must be too small, the lithium abundance in this sightline must exceed the solar-system value (by at least an order of magnitude), or some combination of these factors must apply. Perhaps more plausibly, White's estimate of  $n_e = 0.1 \text{ cm}^{-3}$  implies  $\mathcal{F}^{-1} \approx 380$ , hence  $\delta \approx 0.8$  for a solar-system lithium abundance – that is, little or no depletion of lithium from the gas phase.

#### 5.4 ${}^7\text{Li}/{}^6\text{Li}$ ratios

The column-weighted average isotopic ratio for lithium is insensitive to details of the cloud model (as one might expect since the lines are very optically thin), with  ${}^7\text{Li}/{}^6\text{Li} \approx 1.1 \pm 0.2$  dex for all the solutions presented in Table 1; our adopted solution has  ${}^7\text{Li}/{}^6\text{Li} = 1.12 \pm 0.2$  dex. This value is slightly larger than, but broadly consistent with, the single-cloud results of MHW and LFV, and LFV's claim that their results are insensitive to unresolved structure is therefore supported to the extent that these *average* ratios are in agreement. This averaged result is also extremely close to the meteoritic ratio, 1.09 dex (Anders & Grevesse 1989; Chaussidon & Robert 1998), and therefore stands in contrast to LFV's suggestion that the meteoritic value may be unrepresentative of the ISM value.

#### ACKNOWLEDGMENTS

IAC and RJP are supported by PPARC. We thank the AAT staff for support during the observations. We are grateful to our anonymous referee for insightful and constructive criticisms that led to significant improvements in the paper.

#### REFERENCES

- Alexander J. B., 1967, *Observatory*, 87, 238  
 Anders E., Grevesse N., 1989, *Geochim. Cosmochim. Acta*, 53, 197  
 Barlow M. J., Crawford I. A., Diego F., Dryburgh M., Fish A. C., Howarth I. D., Spyromilio J., Walker D. D., 1995, *MNRAS*, 272, 333  
 Bendali N., Duong H. T., Vialle J. L., 1981, *J. Phys. B*, 14, 4231  
 Cayrel R., Spite M., Spite F., Vangioni-Flam E., Cassé M., Audouze J., 1999, *A&A*, 343, 923  
 Chaussidon M., Robert E., 1998, *Earth Planet. Sci. Lett.*, 164, 577  
 Crawford I. A., 1997, *MNRAS*, 290, 41  
 Crawford I. A., Williams D. A., 1997, *MNRAS*, 291, L53  
 Crawford I. A., Barlow M. J., Diego F., Spyromilio J., 1994, *MNRAS*, 266, 903  
 Ferlet R., Dennefeld M., 1984, *A&A*, 138, 303  
 Israelian G., Santos N. C., Mayor M., Rebolo R., 2001, *Nat*, 411, 163  
 Lambert D. L., Sheffer Y., Crane P., 1990, *ApJ*, 359, L19  
 Le Bourlet J., Gérin M., Pérault M., 1989, *A&A*, 219, 279  
 Lemoine M., Ferlet R., Vidal-Madjar A., 1995, *A&A*, 298, 879 (LFV)  
 Lemoine M., Vangioni-Flam E., Cassé M., 1998, *ApJ*, 499, 735  
 Lynas-Gray A. E., 1993, *Computer Phys. Comm.*, 75, 135  
 Macdonald A. M., ed., 1972, in *Chambers Twentieth Century Dictionary*. Chambers, Edinburgh  
 Meyer D. M., Hawkins I., Wright E. L., 1993, *ApJ*, 409, L61  
 Morton D. C., 1975, *ApJ*, 197, 85  
 Morton D. C., 1991, *ApJS*, 77, 119  
 Nissen P. E., Lambert D. L., Primas F., Smith V. V., 1999, *A&A*, 348, 211  
 Parizot E., 2000, *A&A*, 362, 786  
 Press W. H., Teukolsky S. A., Vetterling W. T., Flannery B. P., 1992, *Numerical Recipes in FORTRAN*. 2nd edn. Cambridge Univ. Press, p. 678  
 Ryan S., Kajino T., Beers T. C., Suzuki T. K., Romano D., Matteucci F., Rosolankova K., 2001, *ApJ*, 549, 55  
 Sansonetti C. J., Richou B., Engleman R., Radziemski L. J., 1995, *Phys. Rev. A*, 52, 2682  
 Shortridge K. et al., 1999, *FIGARO User's Guide* (Starlink User Note 86). CCLRC/Rutherford Appleton Laboratories, Chilton, Didcot  
 Shull J. M., van Steenberg M. E., 1985, *ApJ*, 294, 599  
 Smith V. V., Lambert D. L., Nissen P. E., 1993, *ApJ*, 408, 262  
 Smith V. V., Lambert D. L., Nissen P. E., 1998, *ApJ*, 506, 405  
 Spite M., Spite F., 1982a, *A&A*, 115, 357  
 Spite M., Spite F., 1982b, *Nat*, 297, 483  
 Steigman G., 1996, *ApJ*, 457, 737  
 Steigman G., Walker T. P., 1992, *ApJ*, 385, L13  
 Steigman G., Fields B. D., Olive K. A., Schramm D. N., Walker T. P., 1993, *ApJ*, 415, L35  
 Strömgren B., 1948, *ApJ*, 108, 242  
 Welty D. E., Hobbs L. M., 2001, *ApJS*, 133, 345  
 Welty D. E., Hobbs L. M., Kulkarni V. P., 1994, *ApJ*, 436, 152  
 White R. E., 1986, *ApJ*, 307, 777

This paper has been typeset from a  $\text{\TeX}/\text{\LaTeX}$  file prepared by the author.